

Insertion planning for steerable flexible needles reaching multiple planar targets

Jaeyeon Lee and Wooram Park

Abstract—In this paper, we propose a new insertion plan for steerable flexible needles with which we can target multiple locations in the plane with a single entry point (i.e. port). The method is developed based on the observation that multiple locations can be reached by a flexible needle through insertion, partial retraction, rotation, and re-insertion of the needle. We show that in 2D space this problem can be solved using a geometric relationship between multiple tangent circles. Specifically we find a needle insertion point, a corresponding insertion direction and lengths for insertion and retraction with which we can generate the optimal needle trajectory that reaches two or three planar targets with the minimum tissue damage. This minimization problem is solved using exhaustive search of a cost function on the 1D bounded domain. We build a prototype of a needle insertion system and develop C#-based software to compute the optimal needle paths and perform the planned insertion as an open-loop controller. Finally, actual insertion examples are presented.

I. INTRODUCTION

A long and flexible needle with a bevel tip has been a very interesting research topic for the recent years. Compared to the stiff short needle, this new type of medical needle shows an interesting potential that the user can generate a curved shape of needle trajectory and more importantly, the needle trajectory can be steered by two control inputs: pushing along and rotating around the needle axis. This steerability is hard to achieve with traditional stiff needles.

From the engineering point of view, research on flexible needles includes modeling of kinematics and mechanics, path planning, control, and image-guided needle insertion. Webster III et al. [21] developed a nonholonomic kinematic model for insertion of flexible bevel-tip needles. This model became one of the most popular ones in the research on flexible needles and was adopted in many works (e.g. see [5], [6], [10], [14], [15], [22]). Alterovitz et al. [1] developed a 2D planner for insertion of flexible needles. The needle path which reaches a planar target with the minimized insertion length and simultaneously avoids the obstacles was obtained. Duindam et al. [6] used geometric inverse kinematics to generate a needle path. Park et al. [15] applied the path-of-probability method based on the stochastic model to the needle path generation. Patil and Alterovitz [16] developed a fast planning algorithm for insertion of the flexible needle in 3D environment with obstacles. For control, the LQG control method was applied to flexible needles in [20], where

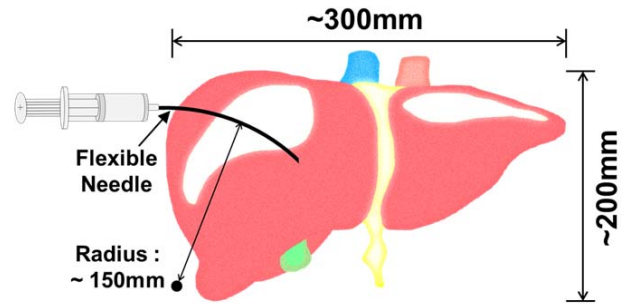


Fig. 1. Illustration of liver biopsy with a flexible needle. The curvature of the needle trajectory is not enough to achieve highly complicated needle path.

the motion uncertainty and sensor types were considered, and optimal placement of sensors were obtained. In addition the arbitrary curvature of the needle trajectory was obtained by duty-cycled spinning. Hauser et al. [8] developed a feedback controller for flexible needles in 3D deformable tissue. Ko et al. [11] developed a needle steering method in 2D with a programmable bevel which enables various curvature of needle trajectories. The fluoroscopic guidance and the ultrasound guidance were shown to be a promising approach for insertion of flexible needles in [7] and [13], respectively. Based on the unicycle model in [21], the needle trajectory can be assumed to be a circular arc when the needle is inserted with pure pushing force along the needle. Even though the simultaneous inputs (i.e. pushing while rotating) can generate complicated needle trajectories, in this paper we split the two inputs to reduce the complexity of the problem as the planar case in [6]. In other words, at a given moment either pushing force or rotation torque is applied at the base of the needle. Therefore, the needle trajectory is a combination of multiple circular arcs which are tangent to each other.

We notice that many path planning methods for flexible needles are based on the assumption that the insertion depth is quite large compared to the radius of curvature of the needle trajectory (e.g. see the simulation results in [5]). Therefore the methods will work with needle trajectories of large curvature (equivalently small radius of curvature), which is possible only in a special situation such as pre-bent needles. Although the trajectory by the pre-bent needle shows small radius of curvature (6.1 cm in [17]), the discontinuity in the trajectory may occur. The curvature of the trajectory of a flexible needle which is the same type of needle used in [21] was estimated as $\kappa = 0.0062 \text{ mm}^{-1}$ in [14], which

Jaeyeon Lee is with the Department of Electrical Engineering, University of Texas at Dallas, 800 W. Campbell Rd., Richardson, TX, USA.

W. Park is with the Department of Mechanical Engineering, University of Texas at Dallas, 800 W. Campbell Rd., Richardson, TX, USA. {jaeyeon.lee, wooram.park}@utdallas.edu

is equivalent to the radius of curvature $R = 161.3$ mm. Realizing that the potential application of the flexible needle includes biopsy and drug delivery, we can assume that the depth of needle insertion is limited by the size of a human body. For example, for the liver biopsy, the needle is inserted from the right side of the abdomen and reaches the inside of the liver as shown in Fig. 1. Therefore, the needle insertion depth does not exceed the depth of the liver. Comparing the radius of curvature of the needle trajectory and the practical insertion depth, we can conclude that very complicated trajectory obtained by a large number of turns of the flexible needle is not practical for needle trajectories whose radius of curvature is large. Furthermore, the short and frequent turns leave much tissue damage and cause the positioning errors.

The task of sequentially reaching multiple locations is a quite traditional problem in robotics [19]. However, while many planning methods for flexible needle insertion from a single fixed point to a single target have been reported, only a few references deal with the multiple-target problem. In [18], it was observed that the flexible needle could reach multiple targets from a single port by inserting, partially retracting, rotating and re-inserting. In [22], the RRT method was used to plan the insertion of multiple needles to multiple targets, but a bounded entry region, not a single port, was considered. Lobaton et al. [12] developed a sampling-based method to generate curvature-constrained paths which can be used for the flexible needle reaching multiple targets.

In our work, we develop an insertion plan for the flexible needle with multiple targets and a single entry point in 2D environment. Because the curvature of the needle trajectory is not large compared to the insertion depth as aforementioned, we assume that the needle trajectory consists of only a few tangent circular arcs. Instead, we allow for selection of the location of the single port for the needle. The optimal choice of the single port location will result in the optimal needle path that reaches multiple targets from the single port and minimizes tissue damage. Our approach is also tested with the experimental setup. The potential application of the proposed approach includes percutaneous biopsy of multiple locations and prostate brachytherapy.

II. PROBLEM STATEMENT

In 2D, two target points can be reached by the flexible needle (see Figure 1 in [18]). The needle hits the first target along the circular arc. Then the needle is retracted up to a special turning point. Next the needle is rotated around the needle axis by 180° at the base. The subsequent insertion will generate a new direction of trajectory which reaches the second target. The tissue damage can be quantified by the length of the needle trajectory inside the tissue, since the tissue damage mainly occurs when the needle travels forward, and the tissue damage is negligible when the needle is retracted. The needle rotation (or turn) can damage the issue, but this is not included in our damage estimation because in our method the number of turns is respectively fixed at 1 and 2 for two targets and three targets.

Our first task is to derive the equation for the cost function which measures the tissue damage when the aforementioned insertion procedure is applied. This cost function is defined as a function of the port location (i.e. initial insertion location). With the input port location, the cost function will compute the length of the needle trajectory after the needle trajectory from the input location to the multiple targets is geometrically obtained. Again, the multiple targets are hit by the needle through insertion, retraction, rotation (or turn) and re-insertion.

We will find the cost functions for a two-target case and a three-target case. Then we will find the optimal port location numerically, and then find the insertion parameters such as the insertion directions and the insertion/retraction lengths. We will perform the actual needle insertion using hardware setup for needle insertion and software that we made for easy application of the planning method.

The proposed problem in this paper can be understood as a Steiner tree problem [9] where the shortest interconnect is sought for a given set of objects. It is worthwhile to note that most versions of the Steiner tree problem are provably NP-complete. Along this line, the work in [12] may be applied to our problem. However, the major difference is that in our problem the starting location for the needle insertion is sought along with the optimal interconnect. In addition, we will solve this problem with consideration of the practical issues in the needle insertion such as the limitation of the trajectory curvature and the potential positioning errors and tissue damage by too many turns. Finally, our approach will be assessed with the needle insertion experiments.

III. GEOMETRY PROBLEMS AND COST FUNCTION

In this section, we derive the equations for the cost functions which quantify the tissue damage for the two-target case and the three-target case. In addition, we find the equations for the insertion direction and lengths of forward insertion and retraction of the needle for hitting multiple targets.

A. Two-target problem

Fig. 2 shows the geometry of the case where the two target points, $P_1 = (x_1, y_1)$ and $P_2 = (x_2, y_2)$, are reached by the needle in this order. The first trajectory from the insertion point $P_{in} = (x, 0)$ to the first target follows a circle whose center and the radius are O_1 and r , respectively. The insertion angle, θ should be determined so that the needle can reach P_1 following a circular arc. Next the needle is retracted up to the turning point, T_1 and then it is turned by 180° . The needle is inserted again from T_1 and it reaches the second target point P_2 . The cost function is the tissue damage estimated by the length of the needle trajectory:

$$f_2(x) = l_1 + l_2.$$

The subscript in $f_2(x)$ denotes that this cost function is defined in the case of two target points.

Now we will derive the equations for the two angles ψ_1 and ψ_2 shown in Fig. 2. The distances of the first and second

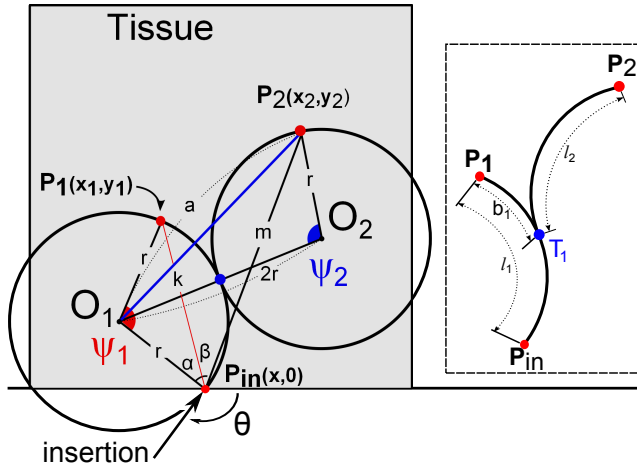


Fig. 2. The two tangent circular arcs show the needle trajectory that reaches two targets.

target points from the insertion point P_{in} are written as

$$k = \sqrt{(x_1 - x)^2 + y_1^2} \quad \text{and} \quad m = \sqrt{(x_2 - x)^2 + y_2^2},$$

respectively. The angles α and β in Fig. 2 are expressed using the lengths as

$$\alpha = \arccos\left(\frac{k}{2r}\right) \quad \text{and} \quad \beta = \arccos\left(\frac{m^2 + k^2 - p_{12}^2}{2mk}\right) \quad (1)$$

where p_{12} is the distance between the two target points. The distance between the center of the first circle, O_1 and the second target, P_2 can be written as

$$a = \sqrt{r^2 + m^2 - 2rm \cos \gamma}$$

where $\gamma = \alpha + \beta$. Consequently the angles ψ_1 and ψ_2 are written as

$$\psi_1 = \arccos\left(\frac{2r^2 - k^2}{2r^2}\right) \quad \text{and} \quad \psi_2 = \arccos\left(\frac{5r^2 - a^2}{4r^2}\right). \quad (2)$$

Therefore the cost function can be rewritten as

$$f_2(x) = l_1 + l_2 = r(\psi_1 + \psi_2) \quad (3)$$

The benefit of this geometric approach is that the coordinates of the centers of the circles and the turning point do not have to be specified. For faster numerical minimization of the cost function, it is good to have the cost function (3) without complicated subroutines that computes the centers and turning points.

Depending on the locations of targets, the solution may not exist. For example, if P_1 is more than $2r$ away from P_{in} or P_2 is more than $3r$ away from O_1 , then there is no solution geometrically. These cases can be automatically detected during the solution process shown above. Specifically the inputs for $\arccos(x)$ should be bounded as $-1 \leq x \leq 1$. If the function inputs in (1) and (2) are outside of this bound, it means that the solution does not exist. Therefore we can filter out the no-solution cases.

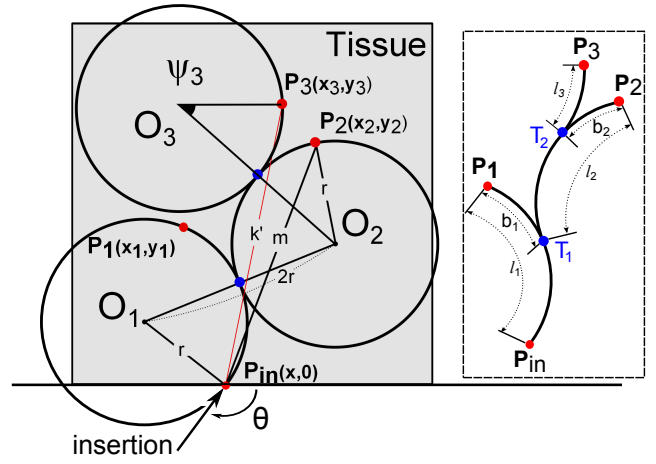


Fig. 3. The three tangent circular arcs show the needle trajectory that reaches three targets.

B. Three-target problem

We can extend the two-target problem to the three-target problem assuming that the targets and the insertion point are on the same plane. Even though this assumption does not reflect the general situation where three targets and a port are not on the plane, this approach is meaningful for multiple reasons.

First, for some potential applications such as prostate brachytherapy [4] there are many targets and we can group three targets so that the aforementioned assumption is satisfied. This approach can reduce the complexity of the problem by replacing the full 3D problem to the planar problem. A similar (but not the same) approach was introduced in [3]. The authors take subgroups of targets and a straight needle reaches the targets with minimum error. Second, it is worth to experimentally test the feasibility of the proposed approach for three targets. For a set of three targets the optimal port on the same plane will be determined and the results will be used in the needle insertion test in Section V. If the performance of the actual insertion for the three targets is verified with our optimization approach, this will open the possibility that the solution of the three-target problem can be improved in the future without a doubt about the feasibility.

Let us assume that the third target is reached as shown in Fig. 3. After the needle reaches P_2 , it is retracted up to the turning point, T_2 , turned by 180° and then inserted again to hit P_3 . The cost function for this case is written as

$$f_3(x) = l_1 + l_2 + l_3,$$

where l_1 , l_2 and l_3 are arc lengths as shown in Fig. 3. The main task is to quantify l_3 , because l_1 and l_2 were identified in the previous subsection.

The distance between P_{in} and P_3 is written as

$$k' = \sqrt{(x_3 - x)^2 + y_3^2}.$$

In the triangle $\triangle P_2 P_{in} P_3$, the angle $\beta' \equiv \angle P_2 P_{in} P_3$ can be

expressed as

$$\beta' = \arccos\left(\frac{k'^2 + m^2 - p_{23}^2}{2k'm}\right),$$

where p_{23} is the distance between P_2 and P_3 . Since the angle $\angle O_1P_{in}P_2$ is given as $\gamma = \alpha + \beta$ as shown in the previous subsection, we have $\alpha' \equiv \angle O_1P_{in}P_3 = \gamma - \beta'$. In $\Delta O_1P_{in}P_3$, we can compute the length,

$$a' \equiv \overline{O_1P_3} = \sqrt{r^2 + k'^2 - 2rk' \cos \alpha'},$$

with which we can compute the angle:

$$\delta \equiv \angle P_3O_1O_2 = \eta_1 + \eta_2$$

where $\eta_1 \equiv \angle P_3O_1P_2$ and $\eta_2 \equiv \angle P_2O_1O_2$. The η_1 and η_2 are written as

$$\eta_1 = \arccos\left(\frac{a'^2 + a^2 - p_{23}^2}{2a'a}\right)$$

$$\eta_2 = \arccos\left(\frac{4r^2 + a^2 - r^2}{4ra}\right).$$

Now let us consider $\Delta O_1O_2P_3$. The length in the triangle can be written as

$$\epsilon \equiv \overline{O_2P_3} = \sqrt{4r^2 + a'^2 - 4ra' \cos(\delta)}.$$

Therefore the angle $\angle O_2O_3P_3$ can be computed as

$$\psi_3 = \angle O_2O_3P_3 = \arccos\left(\frac{5r^2 - \epsilon^2}{4r^2}\right).$$

Finally the cost function is given as

$$f_3(x) = l_1 + l_2 + l_3 = r(\psi_1 + \psi_2 + \psi_3) \quad (4)$$

Like the two-target problem, the function inputs for $\arccos(x)$ can be used to filter out the no-solution cases.

C. Insertion direction and retraction lengths

Even though the insertion direction (angle θ) and retraction lengths (b_1, b_2) in Fig. 2 are not used when the cost function is derived, they should be found after the cost function is minimized because they will be used for actual needle insertion. For a two-target problem, the needle is inserted at the optimal insertion point (P_{in}) with the insertion direction (θ). When the needle inserted forward with the insertion length l_1 , the needle hits the first target. Then it is retraced by b_1 and rotated by 180° at the base. Finally it is reinserted by l_2 to reach the second target.

The coordinates of the point $O_1 = (x_{O1}, y_{O1})$ can be determined using the two points, P_1 and P_{in} . Because both points are on a same circle around the center coordinates, O_1 , we can write two equations with respect to the circle :

$$\begin{cases} (x_1 - x_{O1})^2 + (y_1 - y_{O1})^2 = r^2 \\ (x - x_{O1})^2 + (y_{O1})^2 = r^2. \end{cases}$$

Therefore, there are two possible coordinates of the O_1 , which is

$$O_1 = \left[\frac{x + x_1 \pm y_1 v}{2}, \frac{y_1 \pm (x - x_1)v}{2} \right],$$

where v is written as

$$v = \sqrt{\frac{4r^2}{(x - x_1)^2 + y_1^2} - 1}.$$

One coordinates of a center can be decided by the second target. Accordingly, the angle (θ) can be obtained by

$$\theta = \frac{\pi}{2} + \arccos\left(\frac{x - x_{O1}}{r}\right). \quad (5)$$

In the two target case ($P_1 \rightarrow P_2$), the turning point(T_1) can be calculated by finding the angle $\zeta_1 \equiv \angle O_1P_2$ which is the angle of the vector $\overrightarrow{O_1P_2}$ from x-axis, and $\zeta_2 \equiv \angle P_2O_1O_2$:

$$\zeta_1 = \arctan\left(\frac{y_2 - y_{O1}}{x_2 - x_{O1}}\right) \quad \text{and} \quad \zeta_2 = \arccos\left(\frac{a^2 + 3r^2}{4ar}\right).$$

The coordinates of the turning point (T_1) is computed as

$$T_1 = [x_{O1} + r \cos(\zeta_1 - \zeta_2), y_{O1} + r \sin(\zeta_1 - \zeta_2)].$$

As a result, the retraction length (b_1) can be derived using $\rho_1 \equiv \angle P_1O_1T_1$ as

$$b_1 = r\rho_1 = 2r \arcsin\left(\frac{\overline{P_1T_1}}{2r}\right). \quad (6)$$

where $\overline{P_1T_1}$ is the distance between P_1 and T_1 .

In the three target case ($P_1 \rightarrow P_2 \rightarrow P_3$), there will be two retraction lengths, b_1 and b_2 . The first retraction length (b_1) can be obtained by the same process for b_1 in the two-target problem. Likewise the second retraction length (b_2) can be similarly computed by calculating the second turning point(T_2). Two angles, ξ_1 and ξ_2 , mean $\angle P_3O_2$ which is the angle of the vector $\overrightarrow{P_3O_2}$ from x-axis and $\angle P_3O_2O_3$ respectively, and can be written as

$$\xi_1 = \arctan\left(\frac{y_{O2} - y_3}{x_{O2} - x_3}\right) \quad \text{and} \quad \xi_2 = \arccos\left(\frac{\epsilon^2 + 3r^2}{4r\epsilon}\right).$$

The second turning point (T_2) can be expressed as

$$T_2 = [x_{O2} - r \cos(\xi_1 - \xi_2), y_{O2} + r \sin(\xi_1 - \xi_2)].$$

The coordinates of $O_2(x_{O2}, y_{O2})$ can be obtained by the similar process to the O_1 . The retraction length (b_2) can be derived using $\rho_2 \equiv \angle P_2O_2T_2$

$$b_2 = r\rho_2 = 2r \sin\left(\frac{\overline{P_2T_2}}{2r}\right) \quad (7)$$

where $\overline{P_2T_2}$ is the distance between P_2 and T_2 .

It is important to note that the insertion direction (θ) and the retraction lengths (b_1 and b_2) are obtained after the cost function is minimized. Therefore the calculation in this subsection is not repeated in the minimization.

IV. EXPERIMENTAL SETUP AND SOFTWARE DEVELOPMENT

For the systematic experiment where we can apply the needle insertion plan developed in this paper, we set up a prototype of needle insertion system and build software which allows users to pick the targets, automatically computes the needle insertion plan and executes the actual needle insertion.

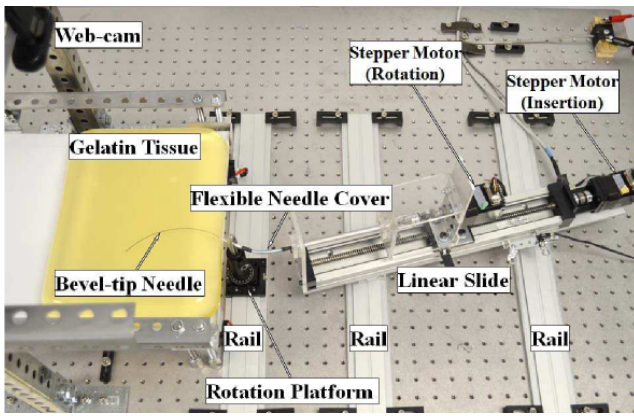


Fig. 4. The hardware setup for needle insertion

A. Hardware

The needle insertion system we set up for experiment is shown in Fig. 4. The system is composed of an operation part and a detection part. The operation part has two stepper motors, which insert and rotate the flexible needle precisely. The stepper motors are operated by a PC via RS-485 and can be rotated by 0.007° for each micro step. One stepper motor attached to the end of a linear motion stage inserts the needle by the desired distance and the other one located on the top of the linear motion stage rotates the needle shaft. A Nitinol wire used as a flexible needle has a 0.71 mm diameter and bevel angle of roughly 45° . There are three straight rails at the bottom of the linear motion stage and a rotation platform, which supports the needle end so that the user can adjust the insertion point and angle manually by aligning the needle with the guide line from the software. We place the linear motion stage at the top of the two straight rails using rotation clamps which allow the stage to slide when the user changes the insertion point and direction. The rotation platform allows the user to precisely set the angle of needle insertion at the resolution of 20 minutes using vernier scale as shown in Fig. 5. In order to prevent unexpected bending during the insertion, a cover material shaped like telescoping support sheath covers the Nitinol wire. In addition, a spring of 6 mm length is equipped between the rotatable needle end and the straight telescoping support sheath as shown in Fig. 5 to prevent the needle bucking and compensate the misalignment between the rotatable end and the straight telescoping support sheath. We make the artificial tissue by mixing clear gelatin sheets with sugar powder in warm water. The detection part consists of a web camera, which can capture 640×480 pixel images at each frame. This web camera is mounted above the artificial tissue about 355.6 mm high position perpendicularly to get the x, y coordinates of needle tip and trajectory effectively. We assume that the top surface of the artificial tissue is the horizontal plane.

B. Software

The insertion procedure is accomplished by motor control software programmed by C# language with visual studio 2010 from Microsoft, in which the image processing is done

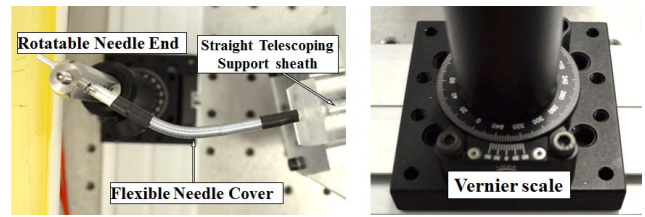


Fig. 5. The flexible needle cover and precision rotation platform

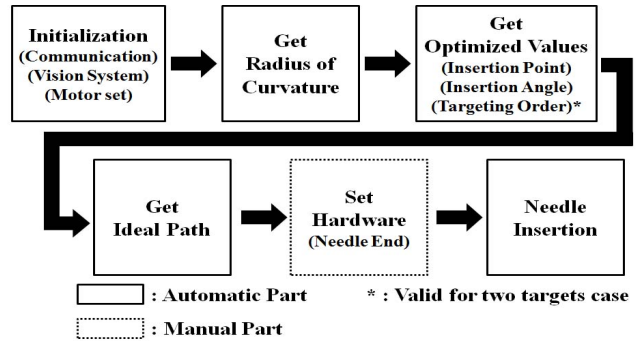


Fig. 6. The block diagram of software operation

by both aforge.NET 2.2.4.1 and EMGUCV 2.4 libraries. The software is composed of several subparts to operate the needle insertion system: *the communication part* to communicate among PC and stepper motors by the results of the insertion plan, *the needle control part* for the user to handle both stepper motors manually, *the vision system part* to detect needle tip, select target points, and watch the optimal needle trajectory, and *the operation part* to calculate the results of the insertion plan. The software operates the needle insertion system by following the procedures shown in Fig. 6. All parameters the software uses are in pixel unit until the final insertion step, in which the final parameters are multiplied by a conversion factor to get the parameters in mm unit. For the constructed hardware system, 1 pixel is converted to 0.4265 mm. Although most processes run automatically by the needle insertion software, the needle setup at the optimal location and direction is done manually. We leave the automation of this process as future work. Before starting each experiment, the software gets the radius of curvature as a preparation step because a radius of curvature can be varied depending on the condition of artificial tissue and environment temperature. The software selects multiple points on the arc of needle trajectory to get the radius of curvature after inserting the needle to a maximum distance on the horizontal plane. In this paper, we developed a method based on [21] in which the author introduced a unicycle model with which the needle trajectory is a circular arc.

V. EXAMPLES OF NEEDLE INSERTION

Experiments are performed to verify the needle insertion plan. The artificial tissue and needle are not replaced during the experiment to maintain consistency in the data and model parameters. We perform three experiment sets with different target points. The target locations are shown in Table I.

*Locations and distances are measured in mm.

Parameters		Two target example		Three target example
		Example 1	Example 2	Example 3
1	Radius	157	124.8	153.1
2	Target points	$P_1(89.1,68.2)$ $P_2(102.4,64.0)$	$P_1(102.4,61.0)$ $P_2(128.8,68.7)$	$P_1(81.0,72.1)$ $P_2(110.5,86.2)$ $P_3(93.8,106.6)$
3	Optimal target sequence	$P_1 - P_2$	$P_2 - P_1$	$P_1 - P_2 - P_3$
4	P_{in} : Optimal insertion point	(109.6,0)	(96.8,0)	(78.9,0)
5	θ : Optimal insertion direction	93.6°	82.7°	74.7°
6	Optimal turning point 1	(106.1,24.6)	(99.6,14.6)	(82.7,18.2)
7	Optimal turning point 2	N/A	N/A	(88.1,41.7)
8	l_1 : Distance for insertion 1	71.9	77.0	72.8
9	b_1 : Distance for retraction 1	47.0	62.1	54.2
10	Turning angle 1	180°	180°	180°
11	l_2 : Distance for insertion 2	39.7	46.7	74.1
12	b_2 : Distance for retraction 2	N/A	N/A	50.0
13	Turning angle 2	N/A	N/A	180°
14	l_3 : Distance for insertion 3	N/A	N/A	65.7
15	Total tissue damage	111.5	123.7	212.6
16	Experiments	Needle tip locations after insertion experiment	$P_1(89.1,67.8)$ $P_2(105.8,66.5)$	$P_1(101.1,61.4)$ $P_2(130.1,68.2)$
			$P_1(80.6,72.5)$ $P_2(111.7,84.4)$ $P_3(92.1,104.5)$	

TABLE I

TARGETS AND OPTIMAL PARAMETERS FOR THE EXPERIMENTS

In the experiments, the order of targets is not fixed before minimization. For Examples 1 and 2 in Table I, the software compares two cases ($P_1 \rightarrow P_2$ and $P_2 \rightarrow P_1$) with respect to the minimum cost and decides the target order which gives a lower cost. Fig. 7 shows the cost function in the bounded search domain for the insertion location. Fig. 7(a) shows the cost functions for Example 1. The two cost function plots for this example are corresponding to the two different target orders ($P_1 \rightarrow P_2$ and $P_2 \rightarrow P_1$). The lower minimum value is found in the continuous line which represents the cost function when P_1 is firstly targeted. Therefore, the minimizer for this cost function becomes the optimal insertion point and the optimal target order is automatically obtained as $P_1 \rightarrow P_2$. Fig. 7(b) shows the cost functions for Example 2. For this case, the lower minimum value appears in the dotted line which represents the cost function when P_2 is firstly targeted. Therefore the optimal target order is $P_2 \rightarrow P_1$. For Example 3, six possible targetting orders are searched. Since the minimization of the cost function developed in Section III is done very fast in a modern PC, searching the six cases is not time-consuming. Through this search, the optimal insertion point and the optimal targetting order are obtained as shown in Table I.

After the insertion point is found by minimizing the cost function, the insertion direction (θ) and the retraction lengths (b_1 and b_2) are simply computed by the method in Section III-C. Note that the needle insertion system only needs the insertion location (P_{in}), the insertion angle (θ) and the traveling lengths: forward insertion lengths (l_1, l_2, l_3) and retraction lengths (b_1, b_2). The numerical results are provided in Table I.

The last row of the Table I shows the locations that the needle actually reaches in the experiment. These locations were measured by the web camera above the artificial tissue. In comparison with the desired target points in the second row of the Table I, the errors are 0.43 mm in minimum

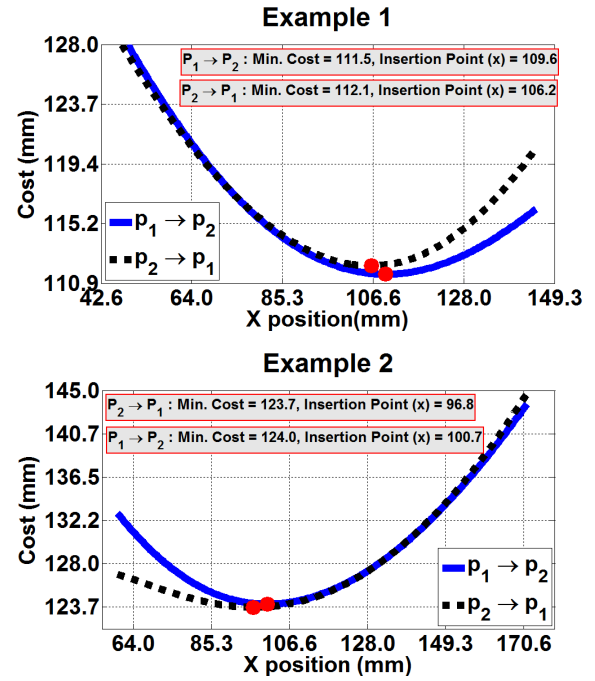


Fig. 7. The costs for the two-target cases

and 2.73 mm in maximum. The source of these errors includes the inaccurate measurement of radius of curvature of the needle trajectory and the manual positioning of the needle tip according to the insertion point and direction calculated from the insertion plan. Nevertheless, it is worth paying attention to the result that the maximum and average errors are respectively less than 3 mm and 2 mm, because the needle was inserted by the open-loop controller and reached multiple targets. The potential source of error in other insertion methods is that the methods allow many turns of the needle as long as a path is generated. In our method, the number of turns is limited. Specifically, the number of turn is $n - 1$ where n is the number of target points. We expect that the needle insertion based on the proposed planning method will become more accurate with the feedback controller which is our future research topic. The result images of the experiments captured by the web camera are represented in Fig. 8. For each case, we can check the actual needle trajectory and target errors during the insertion.

VI. CONCLUSION

A new insertion plan for flexible needles with multiple planar targets and a single entry point was developed. We used the consecutive insertions through insertion, partial retraction, rotation, and re-insertion to target multiple points with the flexible needle. The proposed planning method finds the optimal entry point with which we can generate the needle path which minimizes the tissue damage that is estimated by the length of the needle path. To this end, we defined the cost function which is a function of the port location, and numerically solved the minimization

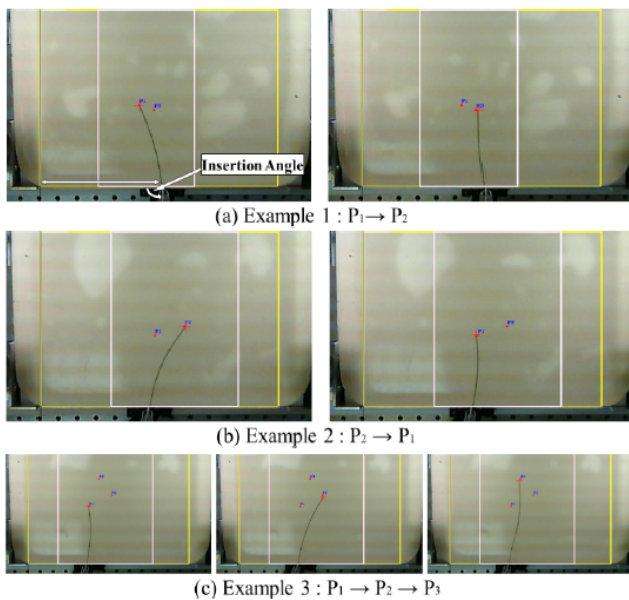


Fig. 8. The examples of experiment

problem. After the minimization, we computed the insertion parameters such as the insertion direction and the lengths for insertion and retraction in addition to the port location.

In order to test the performance of the insertion plan, the hardware was built for the actual needle insertion, and the software was developed for path generation based on the cost minimization and semi-automatic needle control. The experiments showed that the open-loop controller based on the result from the insertion plan could insert the needle to target multiple points with the error less than 3 mm. The averaged error was less than 2 mm. This small error increased the expectation that the needle insertion based on the proposed planner will be very accurate with the feedback control.

Since the experimental setup used the assumption that tissue deformation is negligible and tissue is homogenous, the practical application of the proposed planning requires the test with more practical assumptions and experimental setup. However, this paper provided the significant first step for solving the multiple-target needle insertion problem by proposing a mathematical optimization approach and performing the experimental feasibility test. This provides the new topics for future research such as tests of flexible needle for multiple targets with deformable and inhomogeneous tissue as well as *ex-vivo* and *in-vivo* setup.

The paper focussed on the planar case. As an extended effort, the authors are working on the needle insertion for three-dimensional multiple targets. A journal publication for the theoretical approach is in revision [2], and subsequent experimental results are expected.

REFERENCES

- [1] R. Alterovitz, K. Goldberg, and A. Okamura, "Planning for steerable bevel-tip needle insertion through 2D soft tissue with obstacles," in Proc. IEEE Int. Conf. Robotics and Automation, pp. 1640–1645, 2005.
- [2] O. Bobrenkov, J. Lee, and W. Park, "A new geometry-based plan for inserting flexible needles to reach multiple targets," in *revision*
- [3] E. Dehghan and S.E. Salcudean, "Needle Insertion Parameter Optimization for Brachytherapy," *IEEE Transactions on Robotics*, 25(2):303-315, 2009.
- [4] A.P. Dicker, G. Merrick, L. Gomella, R.K. Valicenti, F. Waterman, *Basic and advanced techniques in prostate brachytherapy*, Informa HealthCare, 2005.
- [5] V. Duindam, R. Alterovitz, S. Sastry, and K. Goldberg, "Screw-based motion planning for bevel-tip flexible needles in 3D environments with obstacles," in Proc. IEEE Int. Conf. Robotics and Automation, pp. 2483–2488, 2008.
- [6] V. Duindam, J. Xu, R. Alterovitz, S. Sastry, and K. Goldberg, "Three-dimensional motion planning algorithms for steerable needles using inverse kinematics," *International Journal of Robotics Research*, 29(7):789–800, 2010.
- [7] D. Glozman and M. Shoham, "Image-guided robotic flexible needle steering," *IEEE Transactions on Robotics*, 23(3):459–467, 2007.
- [8] K. Hauser, R. Alterovitz, N. Chentanez, A. Okamura, and K. Goldberg, "Feedback control for steering needles through 3D deformable tissue using helical paths," in Proc. Robotics: Science and Systems, 2009.
- [9] F.K. Hwang, D.S. Richards, and P. Winter, "The Steiner Tree Problem," *Annals of Discrete Mathematics*, 53, 1992.
- [10] V. Kallem and N.J. Cowan, "Image-guided control of flexible bevel-tip needles," in Proc. IEEE Int. Conf. Robotics and Automation, pp. 3015–3020, 2007.
- [11] S. Y. Ko, Brian L. Davies, F. Rodriguez y Baena, "Two-dimensional needle steering with a "programmable bevel" inspired by nature: Modeling preliminaries," IEEE/RSJ International Conference on Intelligent Robots and Systems, pp. 2319–2324, 2010.
- [12] E. Lobaton, J. Zhang, S. Patil, and R. Alterovitz, "Planning curvature-constrained paths to multiple goals using circle sampling," in Proc. IEEE Int. Conf. Robotics and Automation, pp. 1463–1469, 2011.
- [13] Z. Neubach and M. Shoham, "Ultrasound-guided robot for flexible needle steering," *IEEE Transactions on Biomedical Engineering*, 57(4):799–805, 2010.
- [14] W. Park, K.B. Reed, A.M. Okamura, and G.S. Chirikjian, "Estimation of model parameters for steerable needles," in Proc. IEEE Int. Conf. Robotics and Automation, pp. 3703–3708, 2010.
- [15] W. Park, Y. Wang, and G.S. Chirikjian, "The path-of-probability algorithm for steering and feedback control of flexible needles," *International Journal of Robotics Research*, 29(7):813–830, 2010.
- [16] S. Patil and R. Alterovitz, "Interactive motion planning for steerable needles in 3D environments with obstacles," IEEE RAS & EMBS International Conference on Biomedical Robotics and Biomechanics, pp. 893–899, 2010.
- [17] K.B. Reed, V. Kallem, R. Alterovitz, K. Goldberg, A.M. Okamura, and N.J. Cowan, "Integrated planning and image-guided control for planar needle steering," IEEE RAS & EMBS International Conference on Biomedical Robotics and Biomechanics, pp. 819–824, 2008.
- [18] K.B. Reed, A. Majewicz, V. Kallem, R. Alterovitz, K. Goldberg, N.J. Cowan, A.M. Okamura, "Robot-assisted needle steering," *IEEE Robotics & Automation Magazine*, 18(4):35–46, 2011.
- [19] M. Saha, T. Roughgarden, J.-C. Latombe, and G. Sánchez-Ante, "Planning tours of robotic arms among partitioned goals," *International Journal of Robotics Research*, 25(3):207–223, 2006.
- [20] J. Van Den Berg, S. Patil, R. Alterovitz, P. Abbeel, and K. Goldberg, "LQG-based planning, sensing, and control of steerable needles," *Algorithmic Foundations of Robotics IX*, pp. 373–389, 2011.
- [21] R.J. Webster III, J.S. Kim, N.J. Cowan, G.S. Chirikjian, and A.M. Okamura, "Nonholonomic modeling of needle steering," *International Journal of Robotics Research*, 25(5-6):509-525, 2006.
- [22] J. Xu, V. Duindam, R. Alterovitz, J. Pouliot, J.A.M. Cunha, I.C. Hsu, and K. Goldberg, "Planning fireworks trajectories for steerable medical needles to reduce patient trauma," in Proc. IEEE/RSJ International Conference on Intelligent Robots and Systems, pp. 4517–4522, 2009.